BMC Biology

RESEARCH

Open Access

Ectopic expression of Slc1a2 in the prefrontal cortex of sleep-deprived male mice counteracts the glutamate/GABA-glutamine dysfunction

Fengying Zhang[1,2†], Yao Li[3†], Li Jiang[1,2†], Yingbin Wang[4], Yonghong Tang[1,2], Bo Ouyang[2,5], Guojun Song[6], Xuan Li[7], Xiajie Quan[2,8], Min Li[1,2], Hongying Wang[9], Zhao Pan[1,2], Keyan Chen[10*] and Ping Zhang[1,2*]

Background The prefrontal cortex (PFC) plays a pronounced role in cognitive and emotional functions, which may be compromised by dismal sleep quality. This study intended to clarify the impact of Slc1a2 ectopic expression in the PFC on sleep deprivation (SD)-induced disturbances in the glutamate (Glu)/GABA-glutamine cycle and the role of astrocyte (AC)-neuron (Neu) communication.

Methods Single-cell RNA sequencing was adopted to illuminate cell-specific changes in the brainstem, cortex, and hypothalamus of mice under NS, SD, and post-SD conditions. Cell communication analysis was applied to study interactions between ACs and Neus, which altered after the SD. Slc1a2 was ectopically expressed in the PFC and subjected to SD, followed by electrophysiological, immunofluorescence staining, and [^{1}H-^{13}C]-nuclear magnetic resonance (NMR) assays to examine neural activity and metabolic status. Behavioral tests, including the open field, novel object recognition, and Y-maze, were conducted to examine cognitive functions and emotional states.

Results SD caused notable changes in cellular distribution and downregulation of metabolic and synaptic genes in affected brain regions. Cell communication studies highlighted a reduction in AC-Neu interactions, with corresponding metabolic disruptions in the Glu/GABA-glutamine cycle as depicted by [^{1}H-^{13}C]-NMR results. Behavior tests confirmed anxiety and cognitive deficits in SD mice, which were substantially alleviated by Slc1a2 ectopic expression in the PFC.

Conclusions Slc1a2 ectopic expression in the PFC negates SD-induced GABA dysfunction through vital AC-Neu communication. This study sheds light on the mechanisms through which SD affects neural function and suggesting potential treatments for sleep-related disorders.

Keywords Sleep deprivation, Prefrontal cortex, Slc1a2, Astrocyte-neuron interaction, Glutamate/GABA-glutamine cycle

†Fengying Zhang, Yao Li and Li Jiang are regarded as co-first authors.

*Correspondence:
Keyan Chen
kychen@cmu.edu.cn
Ping Zhang
zhangp-usc@foxmail.com
Full list of author information is available at the end of the article

Background

Sleep disorders are a widespread issue in contemporary society [1], severely impacting both quality of life and physical health, as evidenced by numerous studies [2–4]. Chronic sleep deficiency and sleep deprivation (SD) have been associated with declines in cognitive functions and disruptions in emotional regulation [5, 6]. The prefrontal cortex (PFC), a critical brain region for cognitive and emotional regulation, is essential for maintaining neuropsychological activities, and its functional and structural integrity is crucial [7, 8]. Moreover, the functions of PFC are closely associated with sleep quality, and alterations in sleep quality may directly influence its function [9, 10]. However, the specific mechanisms by which SD affects PFC functions, particularly in terms of neurotransmitter regulation and cellular communication, remain inadequately understood.

Glutamate (Glu) is the primary excitatory neurotransmitter, while gamma-aminobutyric acid (GABA) serves as the primary inhibitory counterpart, and the balance between them is crucial for brain function [11]. SD can lead to an imbalance in Glu and GABA metabolism, affecting neuronal signaling and overall brain function [12]. The Slc1a2 gene, encoding the excitatory amino acid transporter 2 (EAAT2) [13], plays an important role in Glu transport, prominently regulating Glu levels to prevent neurotoxicity caused by its excessive accumulation [14–16]. Our findings indicated that SD might downregulate Slc1a2 expression, leading to Glu/GABA cycle disruptions. Astrocytes (ACs) are vital in maintaining a stable neuronal environment and regulating neurotransmission [17, 18]. They modulate neuronal activity through the uptake and release of neurotransmitters and regulate Glu levels via Slc1a2 [19]. Our research explored how SD affected the interactions between ACs and neurons (Neus) and its impact on PFC function.

The Slc1a2 gene encodes the EAAT2 protein, a highly efficient Glu transporter primarily expressed in ACs [20]. EAAT2 is crucial in clearing Glu from synaptic clefts and preventing Glu-induced neurotoxicity [21]. Research has suggested that Slc1a2 expression is regulated by various factors, including neural activity and inflammatory responses [22, 23]. Furthermore, the downregulation of Slc1a2 is associated with the pathophysiological mechanisms of several neurological diseases, such as epilepsy, neurodegenerative diseases, and stroke [20, 24, 25]. In our study, we explored the expression changes of Slc1a2 under SD conditions and its impact on communication between ACs and Neus through techniques such as single-cell RNA sequencing (scRNA-seq) and cell communication analysis.

This study aimed to investigate how SD affected the function of the Glu/GABA-glutamine cycle in the PFC and to unveil the role of Slc1a2 in this process. We were particularly interested in the changes in communication between ACs and Neus under SD conditions to understand how these interactions affect PFC function. Additionally, this research was expected to provide new theoretical bases and empirical evidence for potential treatments for sleep disorders. We anticipated that this study might unveil how SD altered PFC functions through its impacts on the Glu/GABA-glutamine cycle and intercellular communication, especially between ACs and Neus. Furthermore, we aimed to clarify the specific role of Slc1a2 in regulating these processes and its potential application in ameliorating SD-induced functional impairments in the PFC.

Results

Characterization of cellular transcription profiles in sleep-deprived mice

Wild-type C57BL/6 mice were divided into three groups: an NS control group ($n=3$), a 12-h SD group ($n=3$), and a group allowed 24 h of RS after the SD ($n=3$). scRNA-seq analysis was performed on samples from brain regions closely associated with sleep—cortex, brainstem, and hypothalamus. After the integration of the sequencing data using the "Seurat" package, examination of the cells' gene count (nFeature_RNA), mRNA molecule count (nCount_RNA), and mitochondrial gene percentage (percent.mt) unveiled that the majority of cells had nFeature_RNA < 5000, nCount_RNA < 20,000, and percent.mt < 10% (Fig. S1A).

To ensure data quality, cells displaying 200 < nFeature, RNA < 5000, and percent.mt < 10% were excluded, resulting in an expression matrix comprising 16,827 genes and 20,517 cells. Correlation calculations related to sequencing depth after the filtering indicated a correlation coefficient of − 0.33 between nCount_RNA and percent.mt, and 0.89 between nCount_RNA and nFeature_RNA (Fig. S1B), suggesting high quality in the filtered cellular data.

Subsequently, genes exhibiting high variability were filtered, and the top 2000 variable genes were selected for downstream analysis (Fig. 1A). After normalization, PCA was performed on the selected variable genes to achieve linear dimensionality reduction. Heatmaps of the major genes associated with PC_1–PC_6 were displayed (Fig. S1C), and batch impacts in the sample data were corrected using the "harmony" package (Fig. S1D), prominently mitigating batch influences (Fig. 1B,C). Additionally, PCs were ranked by standard deviation using an Elbow Plot (Fig. 1D), unveiling that PC_1 to PC_20 sufficiently captured the variability within the highly variable genes, thus providing meaningful analysis.

Further dimensionality reduction was conducted using the tSNE algorithm on the first 20 PCs, leading to

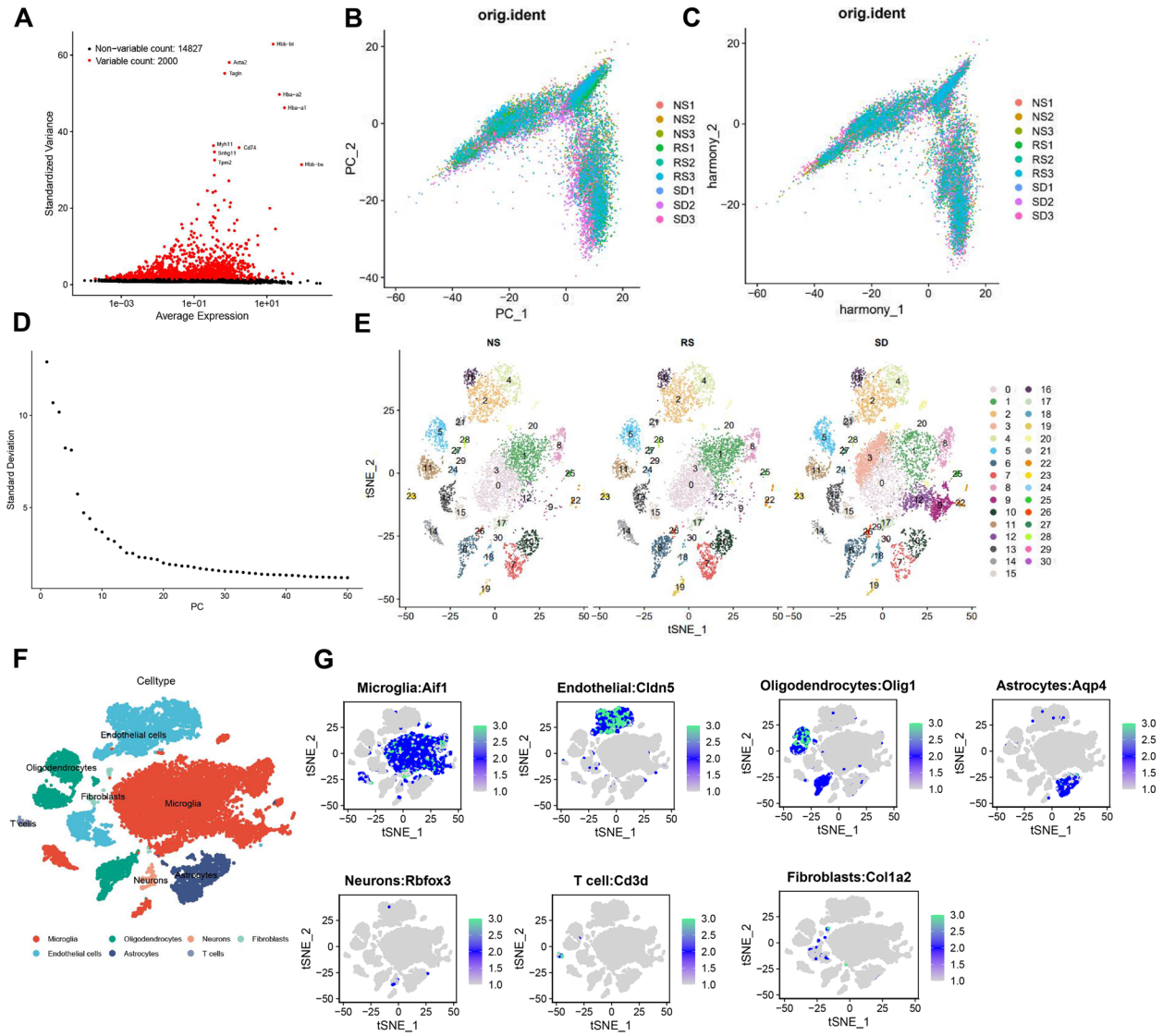

Fig. 1 scRNA-seq detection of brain regions related to sleep across different sleep states in mice. Note: **A** Variance analysis for the selection of highly variable genes, with red representing the top 2000 highly variable genes and black representing genes with low variability, highlighting the names of the top 10 highly variable genes. **B**, **C** Distribution of cells in PC_1 and PC_2 before (**B**) and after (**C**) batch correction with Harmony, where each point represents a cell. **D** Distribution of standard deviations (standard deviation) across principal components (PCs), with important PCs exhibiting greater standard deviations. **E** tSNE clustering visualization presenting a two-dimensional display of cell clustering among the three sample groups, with each color representing a cluster. **F** Visualization of cell annotation results based on tSNE clustering, where each color represents a cell subpopulation. **G** Distribution of marker genes for each cell type, with darker blue indicating higher average expression levels. NS $n=3$, RS $n=3$, SD $n=3$

clustering all cells into 31 clusters (Fig. 1E). These clusters were automatically annotated using the "SingleR" package, identifying seven major cell types: Microglia, ODCs, Neus, Fibroblasts, ECs, ACs, and T cells (Fig. 1F). The distribution of marker genes for these seven cell types was further displayed to validate the accuracy of the annotations (Fig. 1G).

In summary, we successfully identified and annotated seven major cell types through scRNA-seq studies of brain regions associated with sleep in mice under different sleep states.

Central role of ACs in the cellular communication network

Following the detailed annotation and analysis of seven cell types, we delved further into their roles in cellular communication. Initially, a variety of visualization tools and analytical methods were adopted to investigate the communication patterns among these cell types in depth.

Based on the "netVisual_circle" function, a visual chart was generated to illustrate the number and strength of interactions among the seven cell types. The results indicated that most cell types were connected by pronounced links, suggesting that cellular communication was prevalent in our samples (Fig. 2A).

Further, a scatter plot was created using the "netAnalysis_signalingRole_scatter" function to display the signaling capacities of these seven cell types in the cellular communication network. Notably, ACs and ODCs exhibited particularly high activity levels in both sending and receiving signals (Fig. 2B).

To further illuminate their contributions in signal transmission, a heatmap was constructed that confirmed the high activity of ACs, ODCs, and Neus in both receiving and sending signals (Fig. 2C). To understand the communication patterns among these cells, the "identifyCommunicationPatterns" function was used to discern patterns in outgoing signals. This analysis unveiled three main outgoing signal patterns (Patterns) (Fig. S2A-B).

In Pattern 1, ACs, ODCs, and Neus were all highly active, with outgoing signals predominantly enriched in signaling pathways such as PTN, PSAP, MK, VEGF, FGF, EGF, MIF, CXCL, CCL, SEMA3, and WNT (Fig. 2D). These pathways are commonly associated with cellular growth, repair, and inflammation. Similarly, analysis of incoming signal patterns also disclosed three primary incoming signal patterns (Fig. S2C-D), with ACs and Neus showing pronounced activity in Pattern 1. The incoming signals in this pattern were primarily enriched in pathways including PTN, PSAP, MK, PDGF, FGF, EGF, GAS, and EDN, which are also closely related to cellular growth, differentiation, and inflammation (Fig. 2E).

These findings highlighted the key roles of ACs, ODCs, and Neus in the intercellular communication network, particularly in signaling pathways closely associated with cellular proliferation, growth, repair, and inflammation.

Diminished communication among ACs, Neus, and ODCs in sleep-deprived mice

To explore the specificity of cellular communication in sleep-deprived mice, an initial observation was made regarding the proportion of seven cell types in the NS, RS, and SD groups (Fig. 3A). Measurement of cell proportions between groups unveiled that, relative to the NS and RS groups, the proportion of microglia and Neus elevated in the SD group (Fig. 3B, F), while the proportion of ACs and fibroblasts declined (Fig. 3D, H). No pronounced statistical differences were observed in ECs, ODCs, and T cells (Fig. 3C, E, G).

Further analysis of cellular communication across the three groups was visually represented in network diagrams (Fig. 4A). In terms of communication comparison, a pronounced reduction in communication frequency was noted in the SD group relative to the NS and RS groups (Fig. 4B).

Scatter plots illustrated the roles of each cell cluster in the signaling networks of the NS, RS, and SD groups. In the NS group, ACs, Neus, and ODCs predominantly dominated sending and receiving signals. In the RS group, the signal-receiving capacity of ODCs weakened, and in the SD group, the signal-receiving capacity of Neus diminished (Fig. 4C).

Subsequently, ACs, ODCs, and Neus were isolated to compare communication differences among the three groups. The results indicated a pronounced reduction in communication among these three cell types in the SD group compared with the NS and RS groups (Fig. 4D,E; Fig. S3A).

Additionally, the structural and functional similarities among the cell clusters across the three groups were explored, unveiling pronounced differences in the IGF, SEMA3, and VUSFATIN signaling pathways in terms of structure (Fig. S3B) and in the BMP, ANGPTL, and PROS signaling pathways in terms of function (Fig. S3C).

Furthermore, differences in receptor and ligand (L-R) pairs among ODCs, ACs, and Neus across the three groups showed a downward trend in PTN signaling pathway transduction in the SD group (Fig. S3D-F). Violin plots also depicted the expression of the PTN, BMP, and IGF signaling pathways among the seven cell types in the three groups (Fig. S3G-I).

The study unveiled that SD impaired communication among ACs, Neus, and ODCs, thereby impacting essential cellular interactions related to brain function and health.

SD leads to pronounced downregulation of Slc1a2 in mouse ACs in PFC

Following bioinformatics analyses, it was observed that ACs played a dominant role in neuronal communication in sleep-deprived mice. To further investigate how ACs regulate sleep, differential gene expression in ACs was illuminated, comparing the NS group to the SD group, and the RS group to the SD group. Criteria were set at $|\log2FC| > 0.25$ and $p\_val\_adj < 0.05$, unveiling 11 genes upregulated and 100 genes downregulated in the SD group relative to the NS group (Fig. S4A), and 37 genes upregulated and 157 genes downregulated in the SD group relative to the RS group (Fig. S4B).

An intersection of DEGs from both comparisons yielded 56 distinct genes (Fig. 5A). GO and KEGG enrichment study unveiled these genes were primarily enriched in BPs related to the modulation of chemical synaptic transmission and regulation of trans-synaptic signaling (Fig. 5B), CCs such as Neu part and cell junction

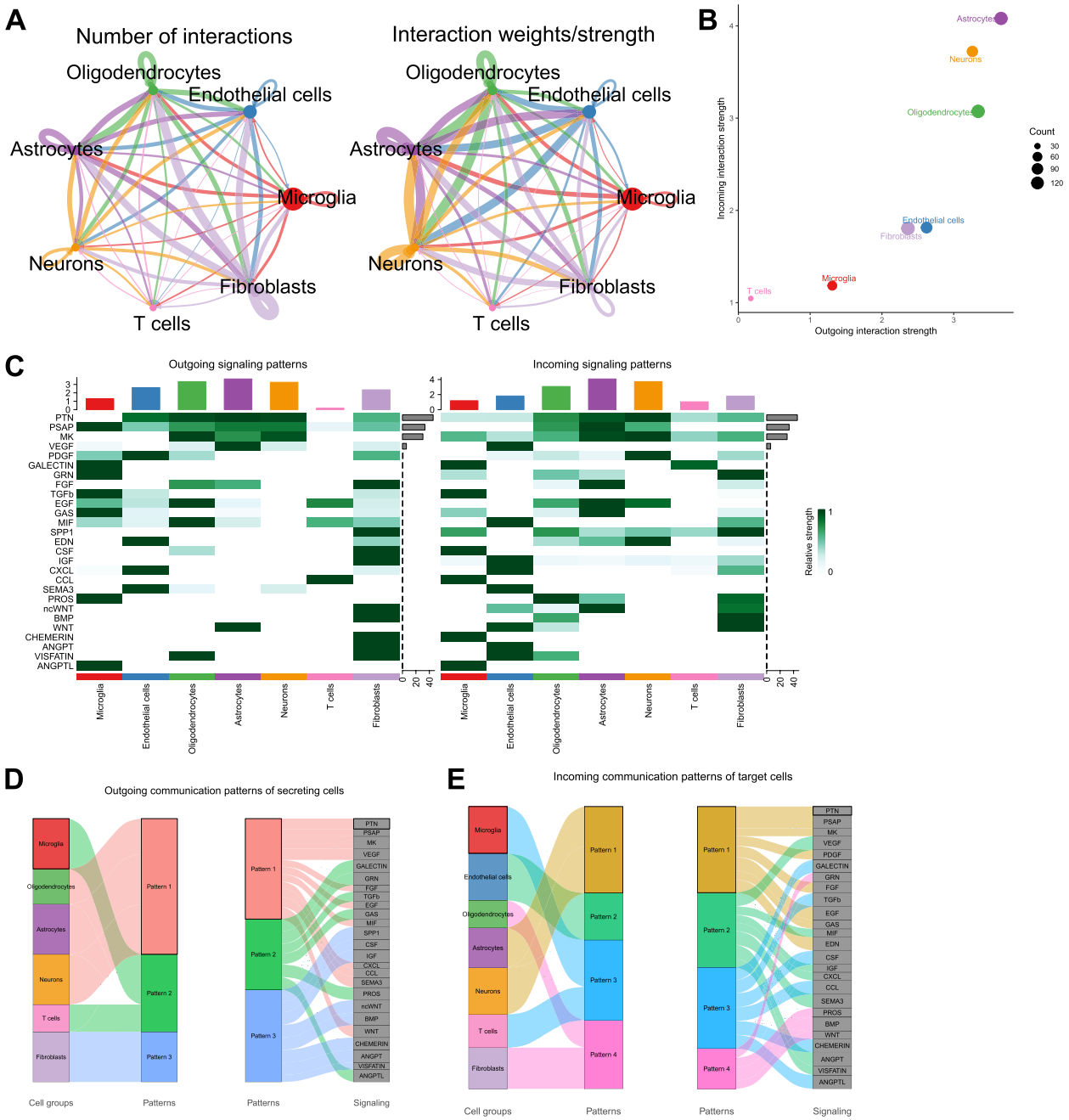

Fig. 2 Detection of communication patterns and main signaling pathways among seven cell types. Note:**A** Visualization generated by the "netVisual_circle" function illustrating the quantity and intensity of interactions among the seven cell types; the size of each circle represents the number or strength of interactions for each cell type, with colors indicating different cell types (red for microglial cells, blue for ECs, green for ODCs, yellow for Neus, dark purple for ACs, pink for T cells, light purple for fibroblasts). Interaction counts are displayed on the left, and interaction strengths on the right. **B** Scatter plot showing the signaling capabilities of the seven cell types within the cellular communication network, with the *x*-axis representing signaling strength sent and the *y*-axis representing signaling strength received. The size of each circle indicates the number of cells. **C** Heatmap displaying the contributions of the seven cell types in signal transmission; the left side illustrates signal-sending patterns, while the right side shows signal-receiving patterns. The color gradient indicates the level of contribution, ranging from low to high. **D** Sankey diagram depicting the primary outgoing signal patterns of the seven cell types and their association with specific signaling pathways, with different colored lines representing different pathways and the width of the lines indicating signal strength. **E** Sankey diagram showing the primary incoming signal patterns of the seven cell types and their association with specific signaling pathways. Different colored lines represent distinct signaling pathways, with line width indicating signal intensity

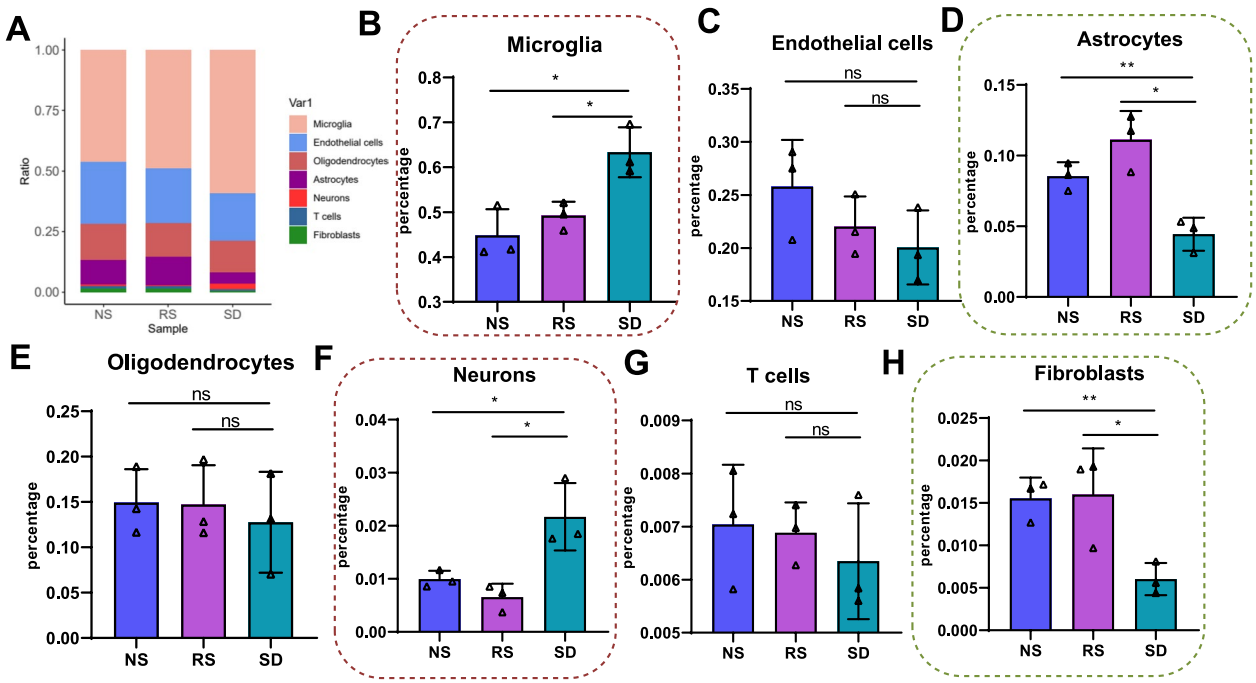

Fig. 3 Detection of cell proportion changes and variabilities in NS, RS, and SD groups. Note: **A** Distribution of seven cell types in NS, RS, and SD groups. **B–H** Differential analyses for microglia (**B**), ECs (**C**), ACs (**D**), ODCs (**E**), Neus (**F**), T cells (**G**), and fibroblasts (**H**) across NS, RS, and SD groups. ns $P > 0.05$, * $P < 0.05$, ** $P < 0.01$

(Fig. S4C), and MFs such as actin-binding and Glu binding (Fig. S4D).

KEGG pathways highlighted pronounced enrichment in amino acid metabolism, synaptic vesicle cycle, and GABAergic synapse (Fig. 5C). A PPI analysis of the proteins encoded by these 56 genes unveiled interactions primarily involved in cholesterol synthesis, immune response, and synaptic transport regulation (Fig. 5D).

Among all these DEGs, Slc1a2 garnered particular attention due to its crucial role in Glu transport and neural signal transmission [26]. Differential analysis results were used to illustrate the distribution of Slc1a2 in ACs across the three groups, unveiling a pronounced decline in Slc1a2 expression in the SD group (Fig. 5E).

To better understand the specific role of Slc1a2 in regulating sleep in ACs, sleep patterns were recorded after the SD treatment. Relative to the NS group, mice in the SD group exhibited facilitated wakefulness and reduced REM and NREM sleep, confirming the success of the SD induction (Fig. S5A-B).

Further analysis involved brain sectioning and IF staining to observe Slc1a2 expression characteristics in ACs within the PFC of SD group mice. It was found that Slc1a2 expression was prominently reduced in the PFC ACs of the SD group mice (Fig. 5F,G). Isolation of the PFC from six mice each in the NS and SD groups, followed by Western blot assay, confirmed these findings, showing a pronounced downregulation of the Slc1a2-encoded protein, EAAT2, in the SD group (Fig. 5H).

The bioinformatics and experimental findings determined that SD caused a pronounced downregulation of Slc1a2 in the ACs of the mouse PFC, impacting crucial aspects of neural function and signaling.

Inhibition of Slc1a2 elevates wakefulness and reduces NREM and REM sleep durations in mice

Previous studies have established that SD suppresses the expression of Slc1a2 in the ACs of the mouse PFC. To delve deeper into the role of Slc1a2 in sleep regulation, gene silencing of Slc1a2 was performed. After a recovery period of 2 weeks, continuous sleep–wake behavior was recorded in mice. Over a 12-h period, the hourly wakefulness of each group was documented. It was found that mice with silenced Slc1a2 exhibited a noticeable elevation in wakefulness relative to mice treated with sh-NC. Quantification unveiled that in every 3-h interval, the total wakefulness, frequency of wakefulness episodes, and duration of these episodes elevated in the Slc1a2-silenced group (Fig. 6A).

Quantification was also conducted on the NREM sleep duration within the same 12-h period. Relative to the sh-NC group, the total duration of NREM sleep prominently declined in the Slc1a2-silenced mice, and the number of sleep cycles also reduced, although the

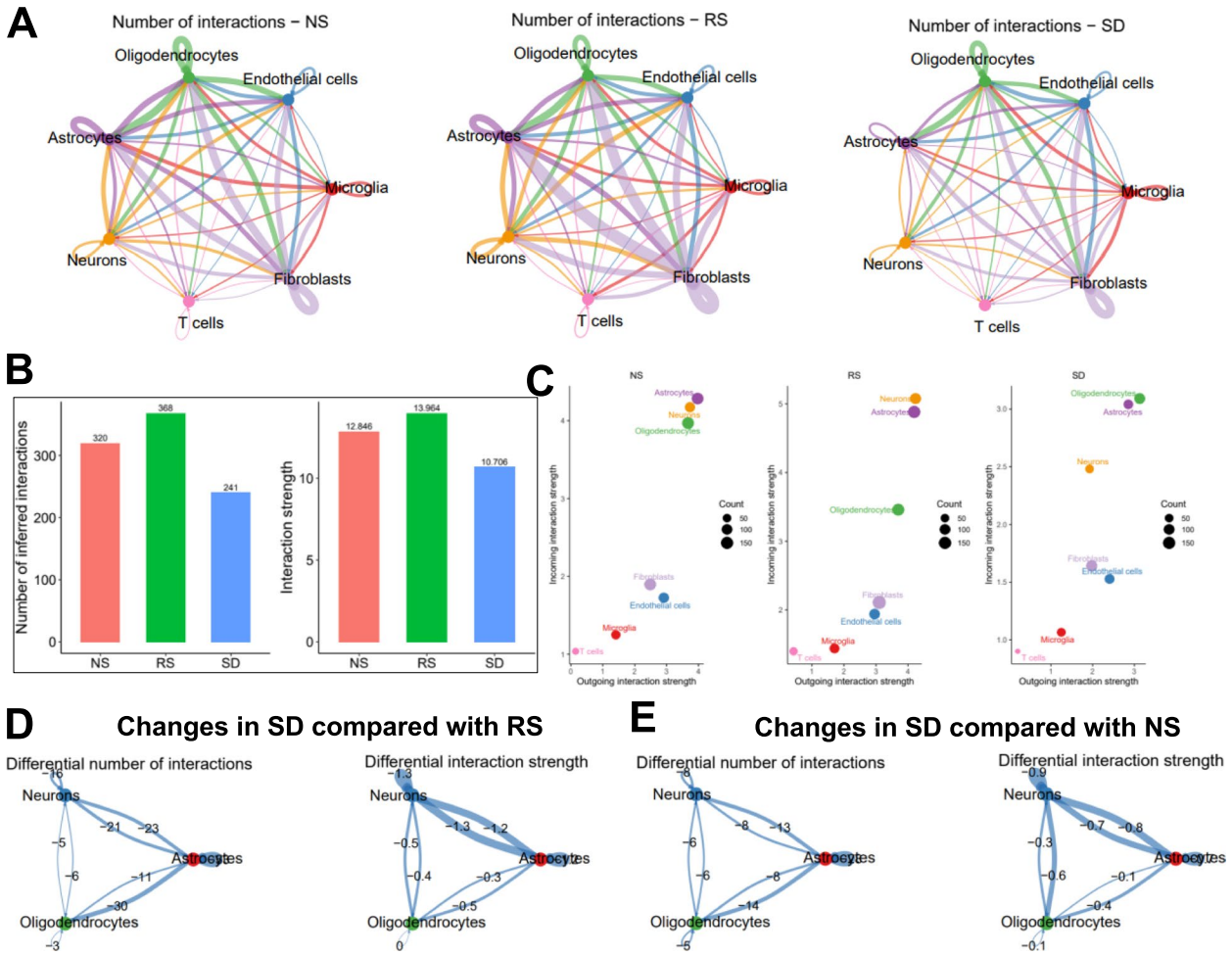

Fig. 4 Comparison of cellular communication among NS, RS, and SD groups and specific cell group signal transmission characteristics. Note: **A** Visualization of the cellular communication networks in NS, RS, and SD groups. **B** Comparison of cellular communication frequency among NS, RS, and SD groups. **C** Scatter plot illustrating the signal sending and receiving capabilities of each cell group in NS, RS, and SD. **D** Differences in communication among ACs, ODCs, and Neus in the SD group relative to the RS group.**E** Differences in communication among ACs, ODCs, and Neus in the SD group relative to the NS group

duration of each sleep cycle showed no pronounced difference (Fig. 6B). Furthermore, the impacts of Slc1a2 silencing on REM sleep were examined. Relative to the sh-NC group, the total duration of REM sleep prominently declined in the Slc1a2-silenced mice, and the number of sleep cycles was reduced, with no pronounced change in the duration of each cycle (Fig. 6C).

In summary, silencing Slc1a2 in the ACs of the PFC elevated wakefulness in mice and reduced the total duration and number of cycles of both NREM and REM sleep, though the duration of individual sleep cycles remained unchanged.

Ectopic expression of Slc1a2 reverses SD-induced abnormalities in Glu and GABA metabolism

Previous investigations confirmed the critical role of Slc1a2 in Glu transport and neural signal transduction, essential processes given that Glu and GABA are the primary excitatory and inhibitory neurotransmitters, respectively. The balance between Glu metabolism and GABA synthesis is crucial for brain function [27]. Earlier experiments (Fig. 6) validated the pronounced function of Slc1a2 during sleep, leading to the hypothesis that SD might disrupt this balance by reducing Slc1a2, thus impairing the GABA-glutamine cycle.

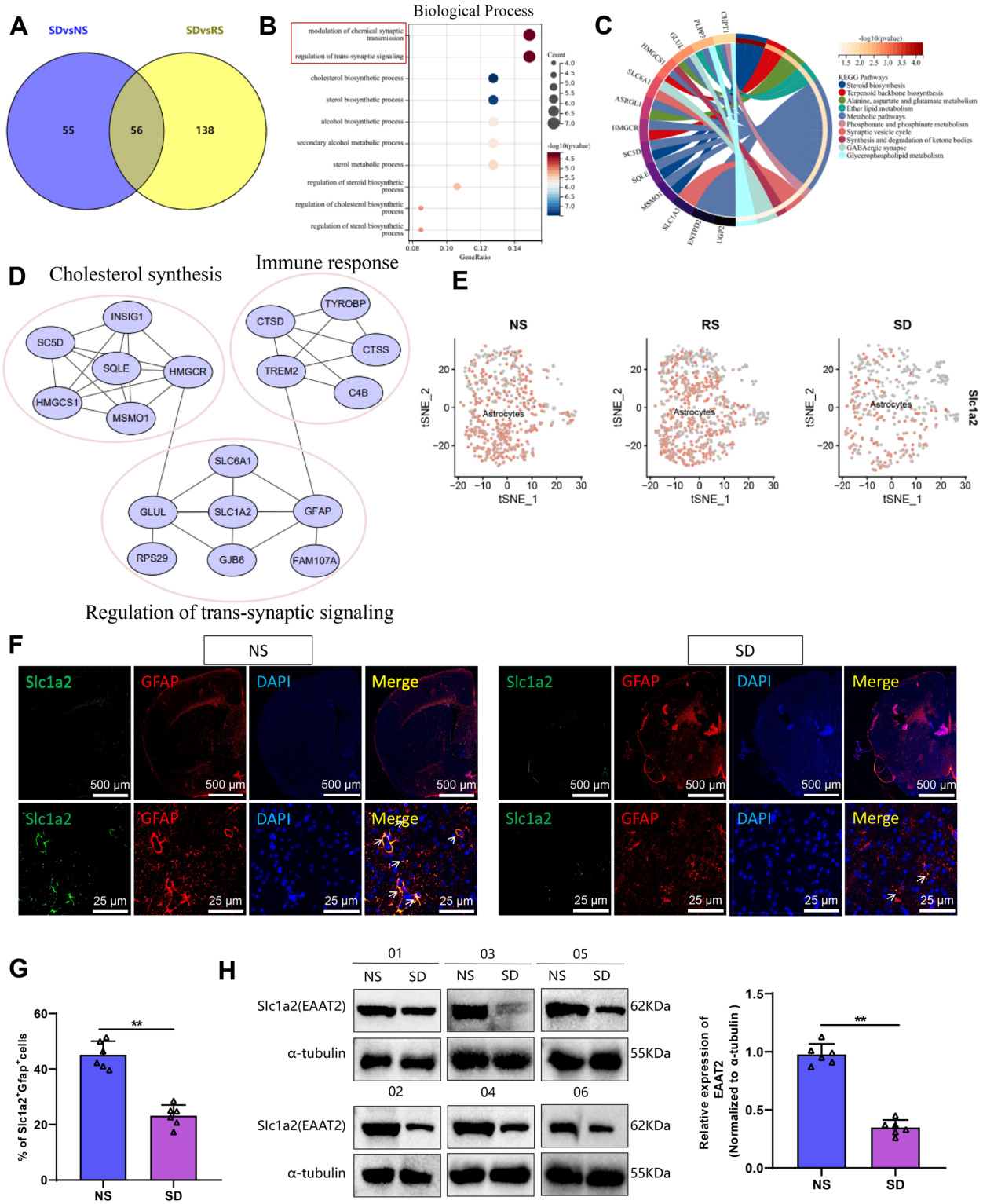

Fig. 5 Gene enrichment in ACs after SD and expression changes of Slc1a2 in the PFC. Note: **A** Intersection of DEGs in ACs of the SD group relative to NS and RS groups.**B** GO enrichment analysis of 56 DEGs in BPs. **C** Enrichment of the 56 DEGs in KEGG pathways. **D** PPI interaction analysis of proteins encoded by the 56 DEGs. **E** Distribution of Slc1a2 expression in ACs across the three sample groups. **F** IF staining of Slc1a2 in ACs from SD group mouse brain tissue. **G** Quantification of Slc1a2-positive cells in ACs of the PFC from image **F**. **H** Western blot analysis of EAAT2 expression in the PFC of mice in the SD and NS groups ($n=6$).** $P<0.01$.$n=6$ mice per group

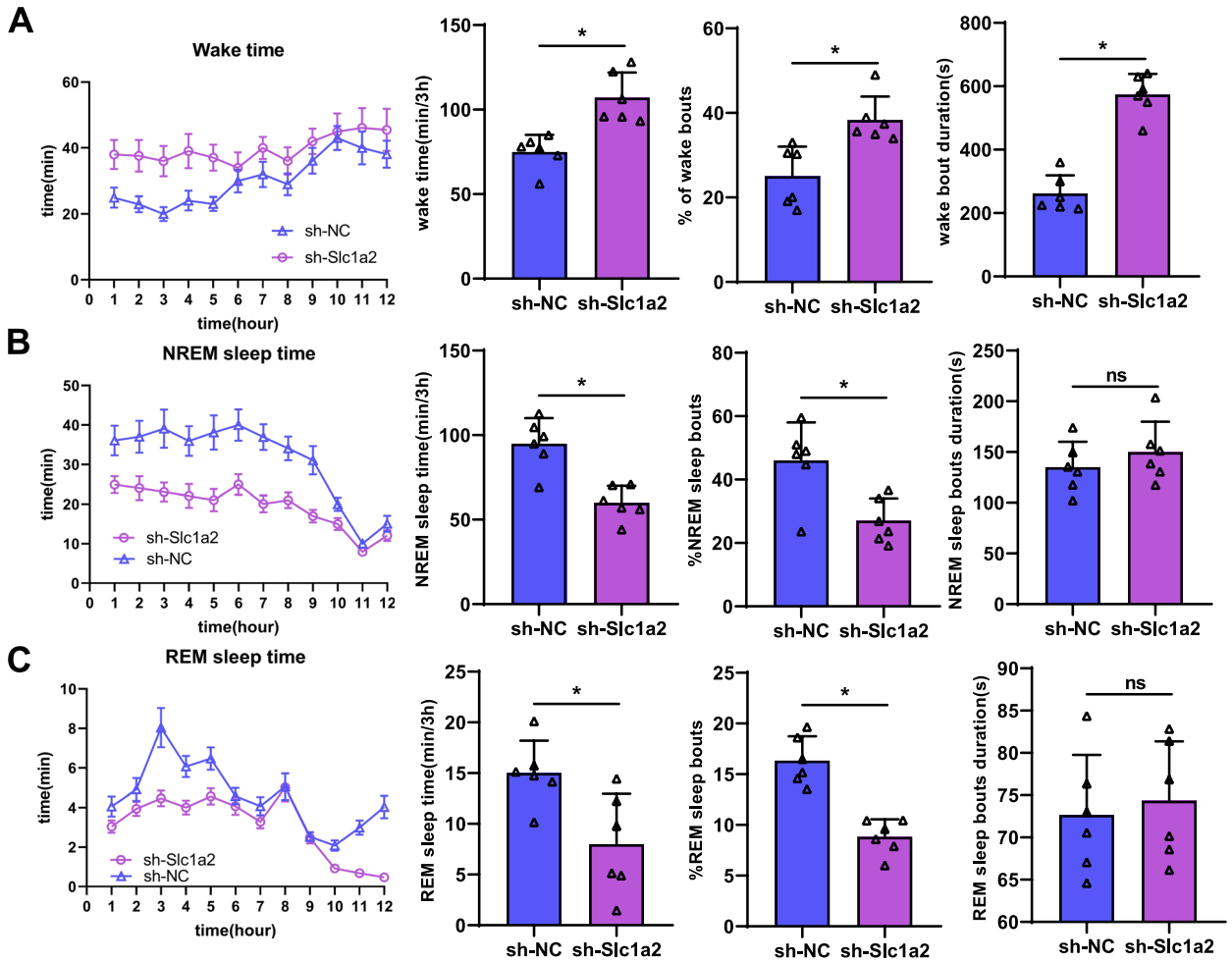

Fig. 6 Detection of sleep–wake behavior in mice following Slc1a2 gene silencing in ACs of the PFC. Note: **A** Detection of wakefulness: Time-series curve showing hourly wakefulness over 12 h, with bar graphs depicting total wakefulness, number of wakefulness periods, and duration of each period every 3 h. **B** Detection of NREM sleep: Time-series curve for hourly NREM sleep over 12 h, with bar graphs showing total duration of NREM sleep, number of sleep cycles, and duration of each cycle every 3 h. **C** Detection of REM sleep: Time-series curve for hourly REM sleep over 12 h, with bar graphs displaying total duration of REM sleep, number of sleep cycles, and duration of each cycle every 3 h. ns $P > 0.05$,* $P < 0.05$.$n = 6$ mice per group

To validate the role of Slc1a2 in Glu metabolism and GABAergic Neu function, Slc1a2 was ectopically expressed in the mouse PFC (Fig. 7A). At 21 days after the AAV infection, the mice were euthanized, and their brains were sectioned for IF staining to examine viral ectopic expression and cellular affinity. The results showed a strong expression of exogenous Slc1a2 in the cell nuclei, with the Slc1a2-eGFP group displaying approximately double the normalized transfection efficiency relative to the control eGFP group (Fig. 7B). Slc1a2 ectopic expression was primarily observed in ACs within the AAV-transduced areas (Fig. 7C).

To explore the metabolic impacts of Slc1a2 on Neus and ACs, metabolic fluxes were examined using ^{13}C-labeled $^{1-13}$C Glucose and $^{2-13}$C Acetate. Then, 30 min after the isotope probe injection, the mice were euthanized, and the PFC was illuminated. Acetate was metabolized only by ACs, while glucose was metabolized by both ACs and Neus as depicted in Fig. 8A. Through the count of carbon atoms labeled, it was found that GABA4, Glu4, and Gln4 were labeled in the first cycle of the TCA cycle in both ACs and Neus; GABA1, GABA2, GABA3, and Glu3, Glu2/Gln2, Gln3/Glu3 (due to overlapping NMR signals of Gln2 and Glu2, Gln3 and Glu3, presented as Glu2/Gln2 and Gln3/Glu3) were labeled in subsequent cycles at different positions. Regarding the metabolism of $^{1-13}$C Glucose in ACs and Neus, it was found that metabolites such as GABA2, GABA3, GABA4, Glu3, Glu4, Gln4, Glu2/Gln2, and Gln3/Glu3 declined after the SD,

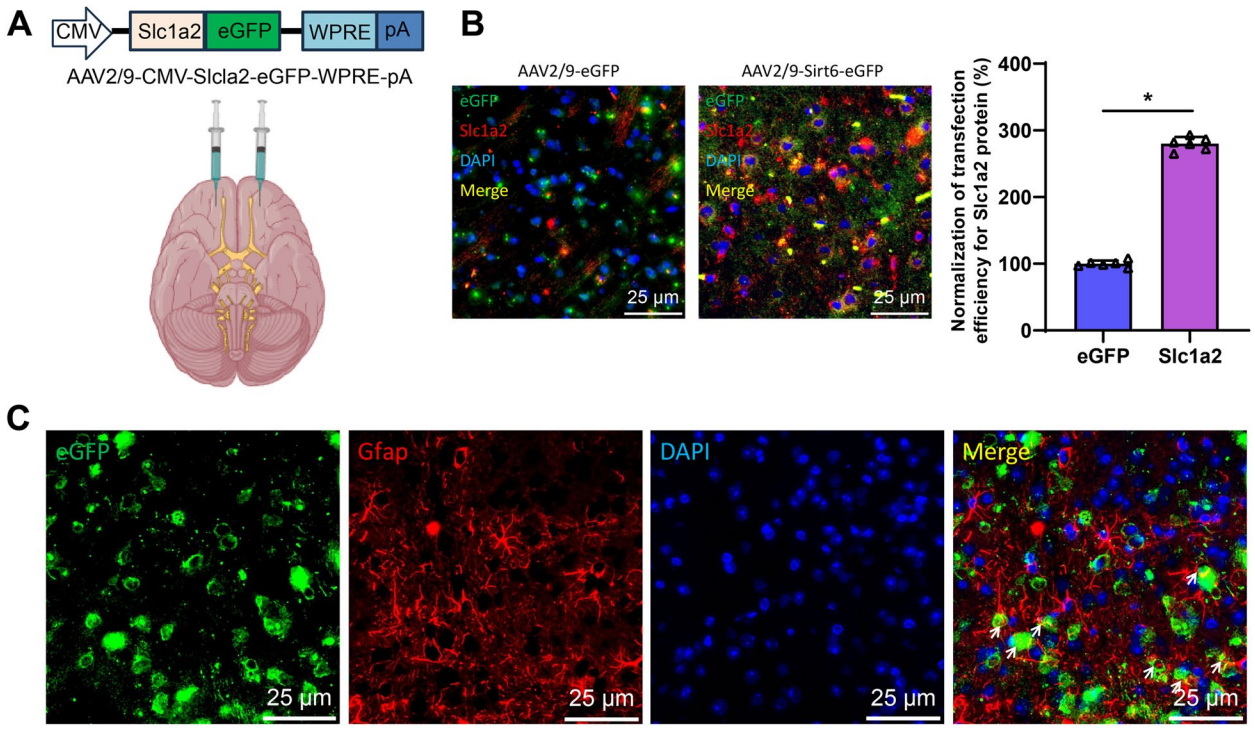

Fig. 7 Ectopic expression impacts of Slc1a2 in the PFC. Note: **A** Schematic of the AAV2/9 adenoviral expression vector used for overexpressing Slc1a2. **B** Comparison of fluorescence intensity in the cell nuclei between exogenous Slc1a2 and control eGFP group. **C** IF staining results showing ectopic expression of Slc1a2 in ACs. $n = 6$ mice per group

while ectopic expression of Slc1a2 in the PFC reversed the reduction of all metabolites except for Glu2/Gln2 (Fig. 8B).

Similar trends were observed for the metabolism of $^{2-13}$C Acetate in ACs, with metabolites GABA2, GABA3, Glu3, Glu4, Gln4, Glu2/Gln2, and Gln3/Glu3 decreasing after the SD, and their reduction being reversed by Slc1a2 ectopic expression in the PFC (Fig. 8C).

Additionally, RT-qPCR provided measurement of the expression of glutamine synthetase (Glul), GABA transporter (Slc6a1/GAT-1), and GABA transaminase (Abat). Results showed that SD prominently reduced the expression of Glul, Slc6a1/GAT-1, and Abat, which was prominently reversed after the Slc1a2 ectopic expression in the PFC relative to the SD + eGFP group (Fig. 8D–F). These findings are consistent with the earlier observed Glu and GABA metabolic outcomes.

Overall, this analysis confirmed that SD adversely affects the metabolic balance of Glu and GABA by suppressing Slc1a2 expression, but ectopic expression of Slc1a2 in the PFC region can reverse these changes, highlighting the critical role of Slc1a2 in regulating neurotransmitter metabolism and maintaining brain function equilibrium.

Ectopic expression of Slc1a2 restores GABAergic Neu function and ameliorates cognitive impairments in sleep-deprived mice

Previous research has delineated that a deficiency of Slc1a2 in the PFC exacerbates sleep disturbances in mice, while its ectopic expression can ameliorate SD-induced abnormalities in Glu metabolism and enhance GABA release. Given GABA's role as the primary inhibitory neurotransmitter in the nervous system, its activity leads to the hyperpolarization of Neus, inhibiting their firing and providing an inhibitory impact across neural networks [28].

Following this, the excitatory synaptic transmission among Neus was examined through EP examination. Relative to the NS + eGFP group, mice in the SD + eGFP group exhibited prominently reduced frequencies and amplitudes of mEPSCs; this reduction was notably reversed in the SD + Slc1a2 group, indicating that SD negatively impacted excitatory synaptic function, which was mitigated by overexpressing Slc1a2 (Fig. 9A).

In the PFC, IF staining for GABA and NeuN was conducted. It was observed that the colocalization of GABA and NeuN prominently declined in the SD + eGFP group, suggesting a detrimental impact of SD on the number or activity of GABAergic Neus in the PFC. However, ectopic

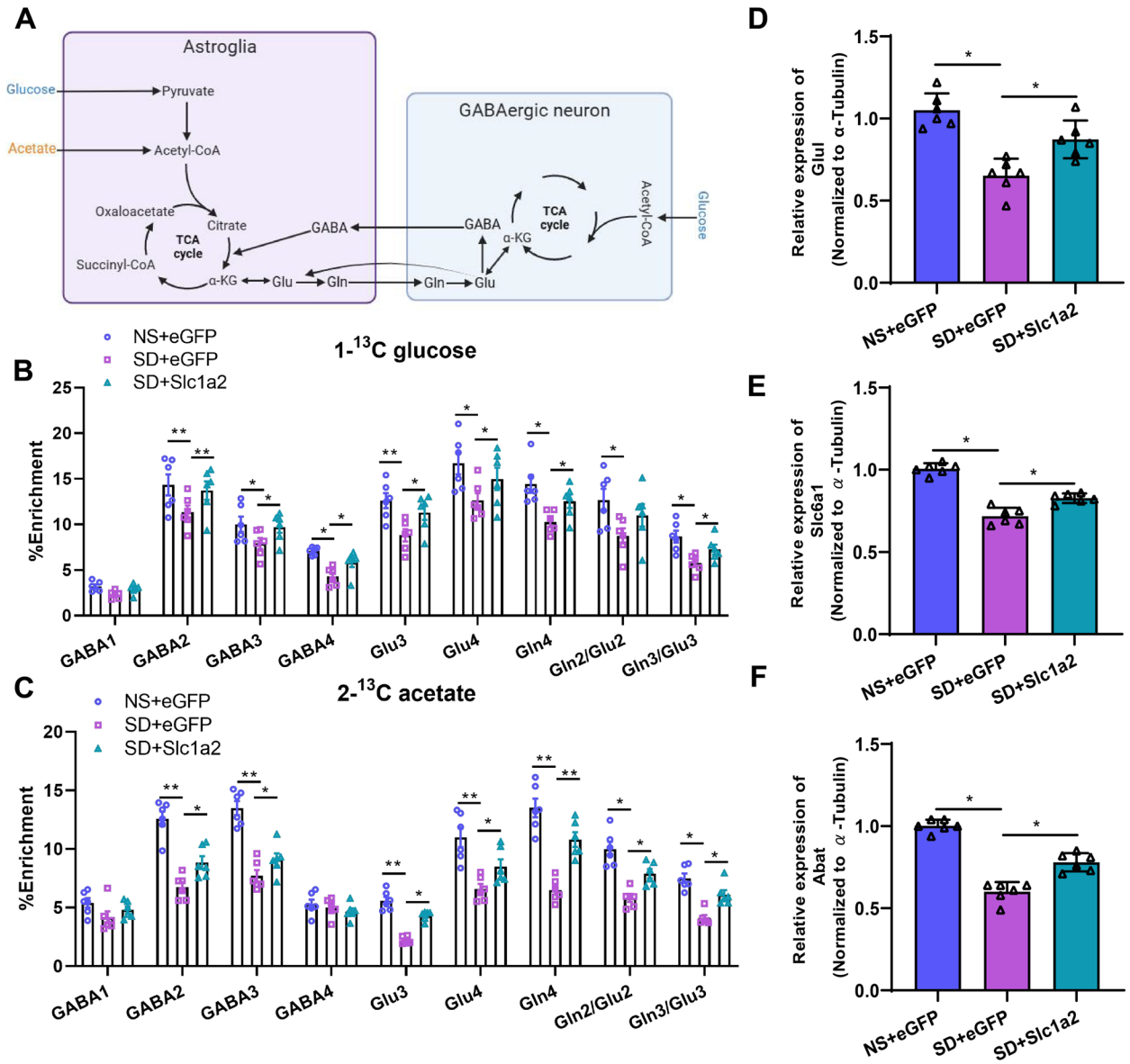

Fig. 8 Impact of Slc1a2 ectopic expression on metabolism in Neus and ACs. Note: **A** Diagram illustrating the metabolic pathways of Glu and GABA and key metabolites involved. **B** Changes in metabolites of $^{1-13}$C Glucose in ACs and Neus. **C** Changes in metabolites of $^{2-13}$C Acetate in ACs; D–F RT-qPCR analysis demonstrating changes in expression of Glul, Slc6a1/GAT-1, and Abat. * $P<0.05$, ** $P<0.01$. $n=6$ mice per group

(See figure on next page.)

Fig. 9 Modulatory impacts of Slc1a2 in the PFC on neurofunctional and cognitive behaviors induced by SD. Note: **A** EP measurement of the frequency and amplitude of mEPSCs in NS + eGFP, SD + eGFP, and SD + Slc1a2 groups of mice. **B** IF detection of GABA and NeuN colocalization in the PFC of the three mouse groups (bar = 50 μm). **C** ELISA results quantifying GABA levels in the CSF of the three groups. **D** Image from the OFT. **E** Quantification of the total distance traveled by mice in the OFT.**F** Quantification of the time spent by mice in the central area of the OFT. **G** Image from the NOR test. **H** Quantification of the recognition index in the NOR test. **I** Quantification of the number of entries to the new object in the NOR test. **J** Results of the YM test. **K** Quantification of the new arm choice index in the YM test. **L** Quantification of the average speed of the three groups of mice. * $P<0.05$,** $P<0.01$.$n=6$ mice per group

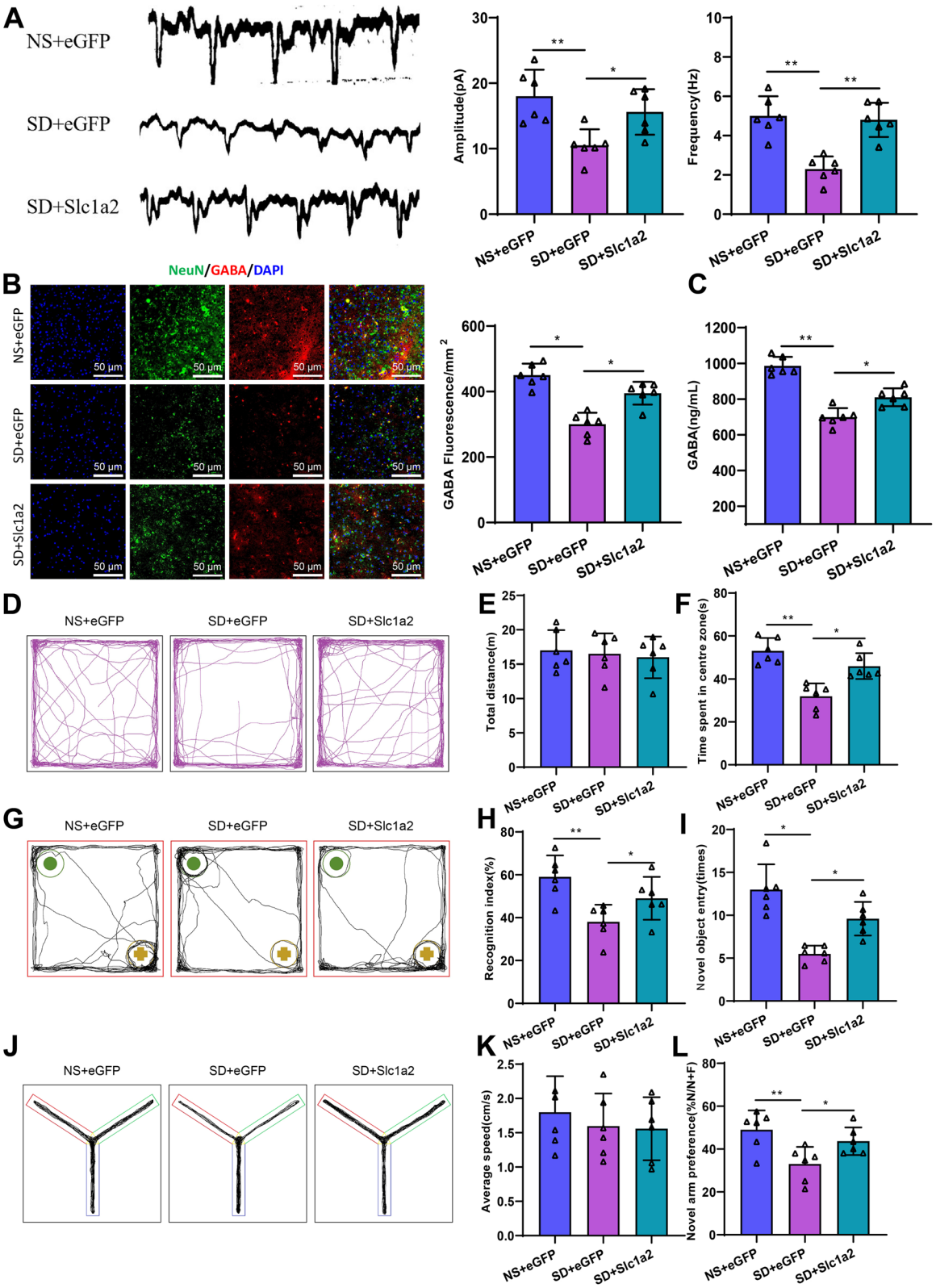

Fig. 9 (See legend on previous page.)

expression of Slc1a2 prominently elevated the colocalization of GABA and NeuN in the PFC relative to the SD + eGFP group, indicating a crucial role of Slc1a2 in regulating the function or quantity of GABAergic Neus in this region (Fig. 9B).

Quantification of GABA in CSF was consistent with these findings, with SD reducing GABA levels, which were restored by overexpressing Slc1a2 (Fig. 9C). These results collectively suggest that Slc1a2 ectopic expression in the PFC crucially supports the normal expression and function of the neurotransmitter GABA.

Behavioral tests were carried out to further investigate the role of Slc1a2 in cognitive impairments induced by SD. In the OFT, neither SD treatment nor Slc1a2 ectopic expression in the PFC affected the mice's locomotor function (Fig. 9D,E). However, mice in the SD + eGFP group spent prominently less time in the center area relative to the NS + eGFP group, suggesting possible cognitive impairment and anxiety behavior induced by SD. This anxiety-like behavior was reversed by overexpressing Slc1a2 in the PFC (Fig. 9F).

Similarly, in the NOR test, the recognition index and the number of entries to a new object were prominently lower in the SD + eGFP group relative to the NS + eGFP group, and these memory process abnormalities induced by SD were mitigated by overexpressing Slc1a2 in the PFC (Fig. 9G–I). Moreover, SD induced spatial memory impairments, as indicated by a reduced new arm choice index in the YM test for the SD + eGFP group relative to the NS + eGFP group. Ectopic expression of Slc1a2 in the PFC inhibited the decline in the new arm choice index, with no pronounced differences in average speed among the three groups (Fig. 9J–L). Overall, these results highlighted that SD disrupted excitatory neural signal transmission and GABAergic Neu function in the mouse PFC, leading to cognitive deficits and anxiety behaviors. However, ectopic expression of Slc1a2 in the PFC counteracted these adverse impacts, thereby maintaining normal cognitive behavior and neurotransmitter GABA functionality.

Discussion

SD is a common challenge that can adversely affect emotional and cognitive functions in individuals [29, 30]. The findings from this study contribute to the development of novel therapeutic approaches by modulating the expression of specific genes like Slc1a2 to alleviate the detrimental impacts of SD. Furthermore, these insights could pave the way for innovative clinical strategies and targets for the treatment of sleep disorders.

Our research delineated that ectopic expression of Slc1a2 in the PFC of male mice prominently reversed the disruptions in the Glu/GABA-glutamine cycle induced by SD. Existing studies suggest that SD impacts neural activities within the brain [31], particularly altering the balance between inhibitory control and brain activation in the PFC area [32]. However, few studies have investigated the underlying genetic changes and regulatory mechanisms involved. Our investigation into the role of Slc1a2 in regulating neurotransmitter balance and protecting neural function provides deeper insights into how SD affects the nervous system and cognitive abilities [33].

Research has suggested that SD affects gene expression and ultrastructure in ACs within the mouse brain, increasing the demand for Glu clearance [34]. Our results align with these findings but go further by showing that ectopic expression of Slc1a2 can prominently reverse these metabolic disruptions, highlighting Slc1a2's central role in maintaining neurotransmitter balance. Our study shed light on the role of communication between ACs and Neus in the context of SD. After inducing SD in model mice, we observed a weakening in the communication between ACs and Neus. SD prominently altered the cell distribution and gene expression in the brainstem, cortex, and hypothalamus.

Behavioral data unveiled that SD mice displayed pronounced anxiety-like behaviors and cognitive impairments. These findings not only validate the adverse impacts of SD on neural functions but also demonstrate the potential of Slc1a2 ectopic expression to improve these behavioral manifestations. These phenotypic studies are consistent with some existing research [35, 36], and our mechanistic studies using scRNA-seq and cellular communication analyses unveiled the critical role played by communication between ACs and Neus in SD mice. The study showed that SD prominently disrupted excitatory neural signal transmission and GABAergic Neu function in the PFC, leading to cognitive impairments and anxiety behaviors. Overexpressing Slc1a2 in the PFC reversed these negative impacts, highlighting the gene's importance in maintaining GABAergic neurotransmitter function and normal cognitive behavior, providing robust theoretical support for further research into sleep disorder treatments (Fig. 10).

Conclusion

In this study, various scientific methods, including scRNA-seq, EP, and IF staining, were applied to delve into the impacts of SD on neurotransmission and cellular interactions within the PFC. The investigation highlighted the crucial role of Slc1a2 ectopic expression in modulating neurological functions and mitigating the negative consequences of SD. Although the results need further clinical verification, they offer substantial insights for advancing neuroscience research.

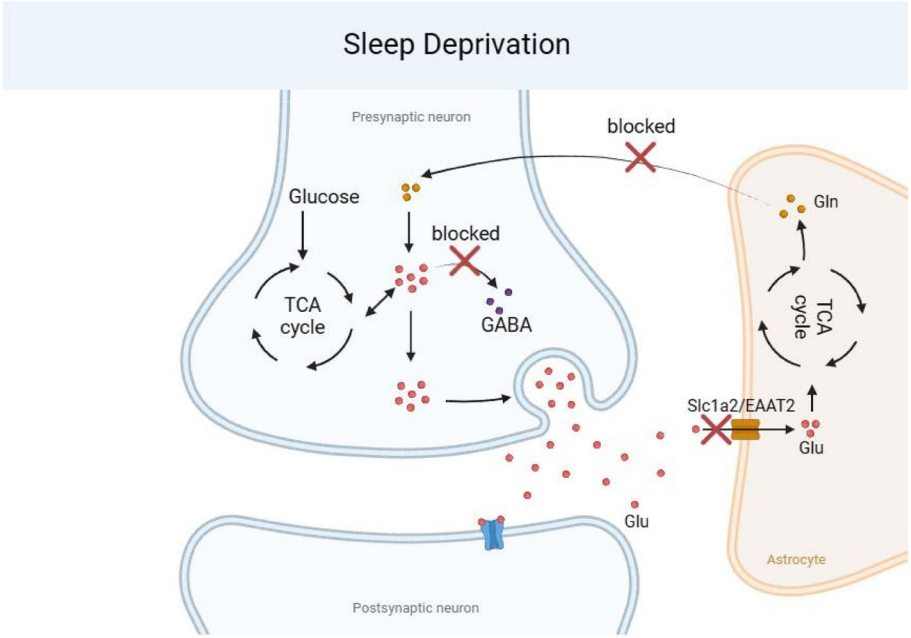

Fig. 10 Mechanistic diagram. The regulatory role of Slc1a2 in the PFC and its critical impact in counteracting SD through the Glu/GABA-glutamine cycle and AC-Neu communication

It is acknowledged that further exploration is needed for some aspects of this study. scRNA-seq provides a detailed gene expression analysis at the individual cell level, but it might miss broader intercellular interactions and physiological responses. The molecular pathways related to Slc1a2, particularly its regulation of neurotransmitters and the subsequent impacts on cognitive and emotional issues induced by SD, are slated for future research. This study reinforces the potential of targeting Slc1a2 modulation as a promising strategy for addressing SD-related conditions.

Methods

Experimental animals

Male C57BL/6J mice were procured from Vital River Laboratory Animal Technology Co., Ltd. (Beijing, China). The mice were raised in a specific pathogen-free (SPF) laboratory environment with cages maintained at a humidity of 60 to 65% and a temperature range of 22 to 25℃. A 12-h light–dark cycle was established, during which the mice had unrestricted access to food and water.

scRNA-seq samples

scRNA-seq samples

The SD mouse model was developed using a rotation-rod-based automated system (Model XR-XS108; Shanghai Xinruan Co., Ltd., Beijing, China) [37, 38], which included a cage where mice could freely access food. The rod at the bottom of the cage rotated both clockwise and counterclockwise. Every six rotations, alternating between three clockwise and three counterclockwise, there was an 18-s pause allowing mice to access food and water. The rod rotated from 20:00 to 08:00 at 5 revolutions per min to prevent sleep. The experimental groups included a normal sleep (NS) group, an SD group, and a group allowed 24 h of recovery sleep (RS) after the SD (Fig. S6). Mice were euthanized by cervical dislocation, and brain regions associated with sleep–wake regulation, such as the brainstem, cortex, and hypothalamus, were rapidly dissected. Tissues from three animals per sleep treatment group and brain region were collected to prepare single-cell suspensions. This study illuminated data from the PFC tissue samples of male C57BL/6J mice using scRNAseq: NS ($n=3$), SD ($n=3$), and RS ($n=3$). Initially, a total of 24,383 cell samples were collected, with specific numbers as follows: NS1 (2001), NS2 (2211), NS3 (2432), RS1 (2207), RS2 (2513), RS3 (3128), SD1 (3470), SD2 (3520), SD3 (2901). After quality filtering based on criteria (nFeature > 200, RNA > 5000, percent.mt < 10%), 20,517 high-quality cells were retained, with specific counts as follows: NS1 (1796), NS2 (1863), NS3 (1889), RS1 (1753), RS2 (2161), RS3 (2437), SD1 (3034), SD2 (3084), SD3 (2500).

scRNA-seq library construction

Tissue samples were processed into single-cell suspensions using papain (P4762, Sigma Aldrich, USA). Single cells were captured using the C1 Single-Cell Auto

Prep System (Fluidigm, Inc., South San Francisco, CA, USA). After capture, cells within the chip were lysed to release mRNA, reverse-transcribed into cDNA. Lysed and reverse-transcribed cDNA underwent pre-amplification within a microfluidic chip to facilitate subsequent sequencing. The amplified cDNA was used for library construction and sequenced on the HiSeq 4000 Illumina platform (parameters: paired-end reads, read length 2×75 bp, approximately 20,000 reads per cell) [39].

Cell annotation

A comprehensive and recognized set of marker genes was used for cell annotation. Neus were marked using NeuN (Rbfox3), Syp, and Syt1. Further classification included excitatory Neus marked with Slc17a7 (VGLUT1), Slc17a6 (VGLUT2), and Camk2a; inhibitory Neus marked with Gad1, Gad2, and Pvalb; ACs primarily marked with Gfap, Aqp4, and Aldh1l1; microglia with Cx3cr1, Aif1 (Iba1), and P2ry12; oligodendrocytes (ODCs) with Mog, Mbp, and Plp1; and endothelial cells (ECs) with Pecam1 (CD31) and Cldn5.

Data quality control

Multiple quality control steps were implemented to ensure data integrity: exclusion of cells with fewer than 200 detected genes or more than 10% mitochondrial gene content. Normalization and linear dimensionality reduction were conducted using principal component analysis (PCA) to ensure robust clustering. Data quality was verified by calculating the correlation between sequencing depth (nCount_RNA) and mitochondrial gene percentage (percent.mt).

scRNA-seq data characterization

Standard downstream processing of scRNA-seq data was conducted using the "Seurat" package (version 3.1) within R software. Genes detected in fewer than three cells, as well as cells with fewer than 200 detected genes, were excluded, and the mitochondrial gene content was restricted to below 10%. Data normalization was performed using the LogNormalize method [40]. Cell clustering was carried out through the "FindClusters" function, and visualization was accomplished using the RunUMAP function. The "FindMarkers" feature of the "Seurat" package was applied to pinpoint specific marker genes for cell clusters by employing the Wilcoxon rank-sum test to compare cells within a cluster against all other cells, identifying differentially expressed genes (DEGs). A Bonferroni-corrected p-value of less than 0.05 was adopted as the threshold for recognizing statistically significant DEGs. Cells were annotated using known lineage-specific marker genes, supplemented by data from the online website CellMarker [41]. Cell communication analysis was conducted using the "CellChat" package in R [41].

Characterization of DEGs

The "clusterProfiler" package, "org.Hs.eg.db" package, "enrichplot" package, and "ggplot2" package in R were used for the enrichment analysis of the identified DEGs, focusing on Gene Ontology (GO) and Kyoto Encyclopedia of Genes and Genomes (KEGG) pathways. Bubble charts were created to display enrichment results for biological processes (BPs), cellular components (CCs), and molecular functions (MFs) in GO, as well as for KEGG pathway analysis.

GO and KEGG enrichment detection

GO and KEGG enrichment analyses of the DEGs were performed using the "clusterProfiler," "org.Hs.eg.db," "enrichplot," and "ggplot2" packages in R. Bubble charts were produced to illustrate the enriched results in the categories of BPs, CCs, and MFs in GO, along with the results from KEGG pathway analysis [42].

Protein–protein interaction (PPI) network node ranking

PPI analysis for proteins encoded by intersectional DEGs was performed using the STRING database (https://string-db.org) with the species condition limited to "Homo sapiens" and the confidence setting at the highest level (0.900). Isolated nodes were excluded, and the default settings were otherwise applied. The results were then imported into Cytoscape 3.7.2 for graphical enhancement.

Electrophysiology (EP) recording and sleep structure detection

Mice were exposed to 1.5–2.5% isoflurane (792,632, Sigma-Aldrich) and positioned in a stereotaxic frame. Four electrode wires were implanted into the cranial surface for electroencephalogram (EEG) recording; two were inserted into the left and right frontal lobes, and the remaining two into the left and right parietal lobes. Additionally, a pair of insulated electrodes was inserted into the neck muscles for electromyogram (EMG) recordings. These electrodes were connected to a microconnector and secured on the cranial surface using dental acrylic resin. After a recovery period of 7 days, brain and muscle electrical activities were recorded using the Medusa small animal EP recording system (Bio-Signal Technologies, Nanjing, China) at a sampling rate of 1000 Hz.

Sleep states were classified into wakefulness, rapid eye movement (REM) sleep, and non-rapid eye movement (NREM) sleep using the Lunion Stage automatic sleep scoring software (LunionData, Shanghai, China). Wakefulness was characterized by EEGs with low amplitude

and high frequency, along with elevated muscle tone. REM sleep was identified by high theta (6–10 Hz) power in the EEG and the absence of muscle strength. NREM sleep was marked by EEGs displaying high voltage and low frequency (1–4 Hz) signals, accompanied by reduced EMG activity [43].

Immunofluorescence (IF) staining

Mice were deeply anesthetized with isoflurane (792,632, Sigma-Aldrich) and sequentially perfused with saline, followed by 4% paraformaldehyde (P0099, Beyotime, Shanghai, China). The entire brain was extracted and fixed in 4% paraformaldehyde for 2 days, then dehydrated in 30% sucrose solution. Brain sections of 40 μm were cut using a Thermo Fisher cryostat (NX50) and stored in an anti-freeze solution at − 20°C. The sections were blocked in PBS containing 0.01% Triton X-100 (P0096, Beyotime) and 10% normal goat serum (C0265, Beyotime). After blocking, sections were incubated overnight at 4°C with primary antibodies: anti-Slc1a2 (ab313454, 1:500, Abcam, UK), anti-Gfap (#56,522, 1:500, CST, USA), anti-NeuN (ab177487, 1:500, Abcam), and anti-GABA (ab86186, 1:200, Abcam). Afterward, sections were washed three times with PBS and incubated for 1 h at room temperature with secondary antibodies Goat Anti-Rabbit IgG H&L (Alexa Fluor® 488) (ab150077, 1:1000, Abcam) and Goat Anti-Rabbit IgG H&L (Alexa Fluor® 594) (ab150080, 1:1000, Abcam). All sections were counterstained with DAPI (C1002, 1:500, Beyotime) for 30 min. Observations were made under a confocal microscope (Leica, STELLARIS 5, Germany).

Western blot protocol

Tissue samples were lysed using RIPA lysis buffer containing 1% PMSF (P0013B, Beyotime) to extract total proteins. The concentration of total proteins in each sample was determined using a BCA Protein Assay Kit (P0011, Beyotime). Based on the molecular weight of the target proteins, SDS–polyacrylamide gels ranging from 8 to 12% were prepared, and equal amounts of protein samples were loaded into the wells using a micro-pipette for electrophoresis separation. Proteins separated on the gel were then transferred onto a PVDF membrane (1,620,177, BIO-RAD, USA) and blocked with 5% non-fat milk at room temperature for 1 h. The membrane was incubated overnight at 4°C with primary antibodies against Slc1a2 (EAAT2) (ab205247, 1:1000) and α-tubulin (ab7291, 1:5000). Following incubation, the membrane was washed several times with 1 × TBST at room temperature, each wash lasting 5 min. Subsequently, an HRP-conjugated Goat Anti-Rabbit IgG (ab6721, 1:2000) secondary antibody was applied, and the membrane was incubated for 1 h at room temperature. The membrane was developed using ECL substrate (1,705,062, Bio-Rad, USA) and imaged on a GE Image Quant LAS 4000C gel documentation system. As normalized to α-tubulin, relative expression levels of the proteins were quantified using ImageJ software (V1.8.0.112).

RT-qPCR protocol

Total RNA from tissues and cells was extracted using Trizol (16,096,020, Thermo, USA). RNA concentration and purity were examined using a Thermo Scientific NanoDrop One/OneC spectrophotometer, achieving an A260/A280 ratio of 2.0 and a concentration greater than 5 μg/μL. The RNA was then converted to cDNA using a First Strand cDNA Synthesis Kit (D7168L, Beyotime). RT-qPCR was performed using a RT-qPCR Kit (Q511-02, Vazyme Biotech, Nanjing) following the manufacturer's protocol. The reaction mixture consisted of 2 μL of cDNA template, 0.2 μL of each forward and reverse primer, 10 μL of RT-qPCR Mix, and the volume was adjusted to 20 μL with RNase-free water. PCR amplification was carried out on a Bio-rad CFX96 Real-Time PCR system. Primer sequences were designed and supplied by Sangon Biotech (Shanghai, China) (Table. S1). Gene expression ratios between the experimental and control groups were calculated using the $2^{-\Delta\Delta}C^{t}$ method, with α-Tubulin as the reference gene.

Viral injection protocol for mouse preconditioning

Seven days before SD treatment, mice were anesthetized intraperitoneally with pentobarbital (45 mg/kg). Each mouse's head was then secured in a stereotaxic frame (RWD Life Science, Shenzhen, China), and an incision was made to expose the skull. Adeno-associated viruses (AAVs) were bilaterally injected into the PFC (AP + 2.5 mm, ML ± 0.4 mm, DV − 1.5 mm) at a rate of 20 nL/min using a 10-μL syringe (Gaoge, Shanghai, China). For the NS + eGFP and SD + eGFP groups, the syringe was pre-loaded with 200 nL of control virus AAV2/9-CMV-bGlobin-MCS-EGFP-WPRE-hGH-polyA for bilateral injection into the PFC. In the SD + Slc1a2 group, the syringe was pre-loaded with 200 nL AAV2/9-CMV-bGlobin-MCS-Slc1a2-EGFP-WPRE-hGH-polyA (titer 7×10^{12} vg/mL; GenChem, Shanghai, China) for bilateral delivery to the PFC. For the sh-NC and sh-Slc1a2 groups, AAVs containing sh-NC and sh-Slc1a2 (CCCTCTTAT CATCTCCAGTTT) sequences were bilaterally injected into the PFC at a rate of 20 nL/min using a 10-μL syringe. Following the injection, the syringe was held in place for an additional 10 min to prevent viral backflow upon withdrawal [44].

Nuclear magnetic resonance (NMR) metabolic evaluation

Metabolic kinetics were examined using [^{1}H-^{13}C]-NMR spectroscopy, employing two types of ^{13}C-labeled substrates, [$^{1-13}$C] glucose, and [$^{2-13}$C] acetate. To reduce the impact of endogenous glucose on ^{13}C labeling, all mice were fasted from 17:00 the day before the experiment. Each mouse was anesthetized with 2.0% isoflurane and infused with the ^{13}C-labeled probe through a PE10 catheter inserted into the tail vein; mice were allowed to move freely for 15 min after the recovery. The ^{13}C-labeled probe was infused at a constant rate for 2 min. After infusion, the mice were allowed free movement in their cages for 30 min, followed by euthanasia. The PFC was harvested, and metabolites were extracted with 60% ethanol. The extracted metabolites were dissolved in phosphate-buffered saline containing sodium 3-(trimethylsilyl)propionate as an internal standard. The supernatant was collected after centrifugation for [^{1}H-^{13}C]-NMR analysis. All samples were illuminated at 25°C using a 500-MHz NMR spectrometer (Bruker BioSpin, Germany). Proton-observed carbon-edited (POCE) spectra differentiated and detected ^{13}C-labeled metabolites across different groups. All NMR data were processed using Topspin commercial software and custom NMR software. Phase and baseline corrections were performed in Topspin and automatically imported into NMR software for peak alignment and integration. The integration of peak areas corresponding to the same regions as pure metabolites was automatically performed using NMR software to calculate the ^{13}C abundance of metabolites [43].

Whole-cell patch-clamp recordings of the PFC

Following anesthesia with isoflurane (792,632, Sigma-Aldrich), mice's brains were rapidly excised and submerged in pre-cooled, oxygenated dissection fluid. Brain slices containing the PFC with a thickness of 300 μm were obtained using a cryostat (Leica VT1000S) in the chilled dissection fluid. The slices were then transferred to an incubation chamber and incubated in artificial cerebrospinal fluid (CSF) at 30°C for 1 h. After incubation, the slices were placed in a recording chamber, and Neus within the PFC region were identified under a microscope for observation. Whole-cell patch clamp recordings were conducted using pipettes (4–8 MΩ, WPI Inc.). Signals were amplified using a MultiClamp 700B amplifier (Molecular Devices). Miniature excitatory postsynaptic currents (mEPSCs) were sampled at a holding potential of − 70 mV in the presence of tetrodotoxin (1 μm) and picrotoxin (100 μm). The pipettes were filled with internal solution, and action potentials were recorded without any synaptic transmission blockers. The number of action potentials induced by each injected current (ranging from 0 to 300 pA, incrementing by 50 pA, duration 500 ms) was calculated, and the frequency (f-I curve) and amplitude of mEPSCs were illuminated using pCLAMP 10.7 software [43].

ELISA for GABA detection

Mice were anesthetized with isoflurane until muscle relaxation was achieved, then positioned laterally on a surgical table. A surgical scalpel was used to expose the spine from the dorsal side, followed by CSF collection through lumbar puncture using a microsyringe. Slowly, 5–10 μL of CSF was drawn. The samples were then transferred to collection tubes and stored at − 80°C for subsequent ELISA [45]. The GABA ELISA Kit (YS02798B, Shanghai Yaji Biotechnology, China) was adopted for the assay. Absorbance was read at 450 nm using a spectrophotometer (Bio-Rad, USA), and a standard curve was plotted to illuminate the data [46].

Behavioral tests

n the open field test (OFT), mice were placed in a square arena divided into quadrants to evaluate their movement and time spent in the central area under standard lighting (800 lx) for 10 min, with movements recorded by a camera positioned 120 cm away [47]. The Y-maze (YM) test involved three arms, where during the training phase, one arm was blocked, and mice could explore the two open arms for 10 min. An hour later, the blocked arm was opened, allowing the mice to explore all three arms for 5 min; this examined their preference for the newly opened arm [48]. Lastly, in the novel object recognition (NOR) test, mice were first acclimated to a setup containing two identical objects for 5 min. After a 2-h interval, one object was replaced with a new one, and the exploration of each object was monitored over another 5-min session to calculate the recognition index and the frequency of new object interactions [43].

Statistical analysis

All data were processed using GraphPad Prism version 8.0. Quantitative data were expressed as mean ± standard deviation (mean ± SD). Comparisons between two groups were performed using unpaired *t*-tests, while comparisons among multiple groups were conducted using one-way analysis of variance (ANOVA). Homogeneity of variance was tested using Levene's test. If variances were found to be equal, pairwise comparisons were made using Dunnett's *t*-test and the least significant difference (LSD-t) test. In cases where variances were not equal, Dunnett's T3 test was adopted. Pearson's analysis was applied to evaluate the correlations between genes as well as between genes and immune cell contents. A *p*-value of less than 0.05 was considered statistically significant, indicating meaningful differences between the datasets.

Abbreviations

AAV	Adeno-associated virus
AC	Astrocyte
CSF	Cerebrospinal fluid
EEG	Electroencephalogram
EMG	Electromyogram
GABA	Gamma-aminobutyric acid
Glu	Glutamate
IF	Immunofluorescence
KEGG	Kyoto Encyclopedia of Genes and Genomes
NMR	Nuclear magnetic resonance
NOR	Novel object recognition
NREM	Non-rapid eye movement (sleep)
NS	Normal sleep
PCA	Principal component analysis
PFC	Prefrontal cortex
REM	Rapid eye movement (sleep)
RNA	Ribonucleic acid
RS	Recovery sleep
SD	Sleep deprivation
SPF	Specific pathogen-free

Supplementary Information

The online version contains supplementary material available at https://doi.org/10.1186/s12915-025-02161-7.

Additional file 1. Fig. S1. Quality Control and PCA Dimensionality Reduction of scRNA-seq Data.

Additional file 2. Fig. S2. Detection of Outgoing and Incoming Signal Patterns.

Additional file 3. Fig. S3. Structural, Functional Similarities, and Key Signaling Pathway Differences Among Cell Groups in NS, RS, and SD Groups.

Additional file 4. Fig. S4. Differential Gene Detection and Functional Annotation in ACs.

Additional file 5. Fig. S5. Impacts of SD on Sleep Stages.

Additional file 6. Fig. S6. Timeline of Model Establishment in NS, SD, and RS Groups.

Additional file 7. Table. S1. RT-qPCR Primer sequence.

Additional file 8. Original WB images.

Acknowledgements
Not applicable.

Authors' contributions
F.Y.Z., Y.L. and L.J. contributed equally to this work and should be considered co-first authors. They performed the experiments, data analysis, and interpretation of results. Y.B.W., Y.H.T., B.O.Y., G.J.S., X.L., and X.J.Q. assisted in the experimental design, data collection, and manuscript preparation. M.L., H.Y.W., Z.P., and L.J. provided critical input in the interpretation of the data and manuscript revision. K.C. and P.Z. supervised the research project, participated in the experimental design, and oversaw the entire study. All authors have read and approved the final version of the manuscript for submission and agree to be accountable for all aspects of the work in ensuring that questions related to the accuracy or integrity of any part of the work are appropriately investigated and resolved.

Funding
This study was supported by National Natural Science Foundation of China (NSFC) (No.82200957), Natural Science Foundation of Hunan Province of China (No.2023JJ30557), Foundation of Health Commission of Hunan Province (No.C202303077734, No.202203074999, No.202203072781) and Project of Hunan Provincial Department of Education (No. 21B0412), Clinical Research 4310 Program of the Affiliated Nanhua Hospital of the University of South China(4310–2021-06), National Key Clinical Specialty Scientific Research Project (grant number:Z2023161) and Hengyang Science and Technology Plan Project (NO.202424017557).

Data availability
All data generated or analysed during this study are included in this published article, its supplementary information files and publicly available repositories. The datasets generated for this study have been deposited in the NCBI Sequence Read Archive (SRA) under BioProject ID PRJNA1161005. The raw sequencing data are available under the following accession numbers: NS group: SRR30666424, SRR30666423, SRR30666422. SD group: SRR30666421, SRR30666420, SRR30666419: RS group: SRR30666418, SRR30666417, SRR30666416.

Declarations

Ethics approval and consent to participate
All animal experiments in this study were completed following the National Institutes of Health Guidelines for the Care and Use of Laboratory Animals established by the National Research Council in 2011. Approval was obtained from the institution's ethics committee (approval number CMUXN2023037).

Consent for publication
Not applicable.

Competing interests
The authors declare no competing interests.

Author details
[1]Department of Neurology, the Affiliated Nanhua Hospital, Hengyang Medical School, University of South China, No. 336, Dongfeng South Road, Zhuhui District, Hengyang, Hunan Province 421001, China. [2]Department of Sleep Medical Centre, the Affiliated Nanhua Hospital,Hengyang Medical School, University of South China, Hengyang, Hunan 421001, China. [3]Department of Physiology, Jinzhou Medical University, Jinzhou 121000, China. [4]Department of Neurosurgery, Central Hospital Affiliated to Shenyang Medical College, Shenyang 110024, China. [5]Department of Traditional Chinese Medicine, the Affiliated Nanhua Hospital, Hengyang Medical School, University of South China, Hengyang, Hunan 421001, China. [6]Department of Radiology, The Affiliated Nanhua Hospital, University of South China, Hengyang, Hunan 421001, China. [7]Department of Docimasiology, Hengyang Medical School, The Affiliated Nanhua Hospital, University of South China, Hengyang 421002, Hunan, China. [8]Department of Information, Affiliated Nanhua Hospital, Hengyang Medical School, University of South China, Hengyang, Hunan 421001, China. [9]Department of Respiratory and Critical Care Medicine, the Affiliated Nanhua Hospital, Hengyang Medical School, University of South China, Hengyang, Hunan 421001, China. [10]Laboratory Animal Science of China Medical University, No.77 Puhe Road, Shenyang, Liaoning 110122, China.

Received: 3 May 2024 Accepted: 14 February 2025
Published online: 26 March 2025

References

1. Vgontzas A, Pavlović J, Bertisch S. Sleep symptoms and disorders in episodic migraine: assessment and management. Curr Pain Headache Rep. 2023;27:511–20.
2. Thabet F, Tabarki B. Common sleep disorders in children: assessment and treatment. Neurosciences. 2023;28:85–90.
3. McLafferty LP, Spada M, Gopalan P. Pharmacologic treatment of sleep disorders in pregnancy. Sleep Med Clin. 2022;17:445–52.
4. Stewart K, Shakarishvili N, Michalak A, Maschauer EL, Jenkins N, Riha RL. Treating sleep disorders following traumatic brain injury in adults: Time for renewed effort? Sleep Med Rev. 2022;63: 101631.
5. Siclari F, Valli K, Arnulf I. Dreams and nightmares in healthy adults and in patients with sleep and neurological disorders. The Lancet Neurology. 2020;19:849–59.
6. Blackmer AB, Feinstein JA. Management of Sleep Disorders in Children With Neurodevelopmental Disorders: A Review. Pharmacotherapy: The Journal of Human Pharmacology and Drug. Therapy. 2016;36:84–98.

7. Hiser J, Koenigs M. The multifaceted role of the ventromedial prefrontal cortex in emotion, decision making, social cognition, and psychopathology. Biol Psychiat. 2018;83:638–47.
8. Shallice T, Cipolotti L. The prefrontal cortex and neurological impairments of active thought. Annu Rev Psychol. 2018;69:157–80.
9. Tossell K, Yu X, Giannos P, Anuncibay Soto B, Nollet M, Yustos R, et al. Somatostatin neurons in prefrontal cortex initiate sleep-preparatory behavior and sleep via the preoptic and lateral hypothalamus. Nat Neurosci. 2023;26:1805–19.
10. Hong J, Lozano DE, Beier KT, Chung S, Weber F. Prefrontal cortical regulation of REM sleep. Nat Neurosci. 2023;26:1820–32.
11. Sears SM, Hewett SJ. Influence of glutamate and GABA transport on brain excitatory/inhibitory balance. Exp Biol Med. 2021;246:1069–83.
12. Yu X, Li W, Ma Y, Tossell K, Harris JJ, Harding EC, et al. GABA and glutamate neurons in the VTA regulate sleep and wakefulness. Nat Neurosci. 2018;22:106–19.
13. Zhou Y, Hassel B, Eid T, Danbolt NC. Axon-terminals expressing EAAT2 (GLT-1; Slc1a2) are common in the forebrain and not limited to the hippocampus. Neurochem Int. 2019;123:101–13.
14. Zhou Y, Wang X, Tzingounis AV, Danbolt NC, Larsson HP. EAAT2 (GLT-1; slc1a2) Glutamate Transporters Reconstituted in Liposomes Argues against Heteroexchange Being Substantially Faster than Net Uptake. J Neurosci. 2014;34:13472–85.
15. Pajarillo E, Digman A, Nyarko-Danquah I, Son D-S, Soliman KFA, Aschner M, et al. Astrocytic transcription factor REST upregulates glutamate transporter EAAT2, protecting dopaminergic neurons from manganese-induced excitotoxicity. J Biol Chem. 2021;297: 101372.
16. Jiang L-L, Zhu B, Zhao Y, Li X, Liu T, Pina-Crespo J, et al. Membralin deficiency dysregulates astrocytic glutamate homeostasis, leading to ALS-like impairment. J Clin Investig. 2019;129:3103–20.
17. Kim N-S, Chung W-S. Astrocytes regulate neuronal network activity by mediating synapse remodeling. Neurosci Res. 2023;187:3–13.
18. Freeman MR. Specification and Morphogenesis of Astrocytes. Science. 2010;330:774–8.
19. Abdolmaleky HM, Martin M, Zhou J-R, Thiagalingam S. Epigenetic Alterations of Brain Non-Neuronal Cells in Major Mental Diseases. Genes. 2023;14: 896.
20. Todd AC, Hardingham GE. The Regulation of Astrocytic Glutamate Transporters in Health and Neurodegenerative Diseases. Int J Mol Sci. 2020;21: 9607.
21. Fontana ACK. Current approaches to enhance glutamate transporter function and expression. J Neurochem. 2015;134:982–1007.
22. Hasel P, Dando O, Jiwaji Z, Baxter P, Todd AC, Heron S, et al. Neurons and neuronal activity control gene expression in astrocytes to regulate their development and metabolism. Nat Commun. 2017;8:15132.
23. Gan Z, Guo Y, Zhao M, Ye Y, Liao Y, Liu B, et al. Excitatory amino acid transporter supports inflammatory macrophage responses. Science Bulletin. 2024;69:2405–19.
24. Qu Q, Zhang W, Wang J, Mai D, Ren S, Qu S, et al. Functional investigation of SLC1A2 variants associated with epilepsy. Cell Death and Disease. 2022;13:13.
25. Yang Z-B, Zhang Z, Li T-B, Lou Z, Li S-Y, Yang H, et al. Up-regulation of brain-enriched miR-107 promotes excitatory neurotoxicity through down-regulation of glutamate transporter-1 expression following ischaemic stroke. Clin Sci. 2014;127:679–89.
26. Briggs C, Hirasawa M, Semba K. Sleep Deprivation Distinctly Alters Glutamate Transporter 1 Apposition and Excitatory Transmission to Orexin and MCH Neurons. J Neurosci. 2018;38:2505–18.
27. Andersen JV, Schousboe A, Verkhratsky A. Astrocyte energy and neurotransmitter metabolism in Alzheimer's disease: Integration of the glutamate/GABA-glutamine cycle. Prog Neurobiol. 2022;217: 102331.
28. Tritsch NX, Granger AJ, Sabatini BL. Mechanisms and functions of GABA co-release. Nat Rev Neurosci. 2016;17:139–45.
29. Krause AJ, Simon EB, Mander BA, Greer SM, Saletin JM, Goldstein-Piekarski AN, et al. The sleep-deprived human brain. Nat Rev Neurosci. 2017;18:404–18.
30. Kang Z, Lin Y, Su C, Li S, Xie W, Wu X. Hsp70 ameliorates sleep deprivation-induced anxiety-like behavior and cognitive impairment in mice. Brain Res Bull. 2023;204: 110791.
31. Roschel H, Gualano B, Ostojic SM, Rawson ES. Creatine Supplementation and Brain Health. Nutrients. 2021;13: 586.
32. Zhao R, Zhang X, Fei N, Zhu Y, Sun J, Liu P, et al. Decreased cortical and subcortical response to inhibition control after sleep deprivation. Brain Imaging Behav. 2018;13:638–50.
33. Peterson AR, Garcia TA, Cullion K, Tiwari-Woodruff SK, Pedapati EV, Binder DK. Targeted overexpression of glutamate transporter-1 reduces seizures and attenuates pathological changes in a mouse model of epilepsy. Neurobiol Dis. 2021;157: 105443.
34. Bellesi M, de Vivo L, Tononi G, Cirelli C. Effects of sleep and wake on astrocytes: clues from molecular and ultrastructural studies. BMC Biology. 2015;13:1–7.
35. Zhai S, Yin M, Sun H, Jiang X, Liu Y, Marshall C, et al. The day-night differences in cognitive and anxiety-like behaviors of mice after chronic sleep restriction. FASEB J. 2023;37(7):e23034.
36. Li J, Zhang H, Deng B, Wang X, Liang P, Xu S, et al. Dexmedetomidine Improves Anxiety-like Behaviors in Sleep-Deprived Mice by Inhibiting the p38/MSK1/NFκB Pathway and Reducing Inflammation and Oxidative Stress. Brain Sci. 2023;13: 1058.
37. Atrooz F, Liu H, Kochi C, Salim S. Early Life Sleep Deprivation: Role of Oxido-Inflammatory Processes. Neuroscience. 2019;406:22–37.
38. Zhang S, Zhang Y, Zheng Y, Zhu S, Sun J, Deng Y, et al. Dexmedetomidine attenuates sleep deprivation-induced inhibition of hippocampal neurogenesis via VEGF-VEGFR2 signaling and inhibits neuroinflammation. Biomed Pharmacother. 2023;165: 115085.
39. Keefe F, Monzón-Sandoval J, Rosser AE, Webber C, Li M. Single-Cell Transcriptomics Reveals Conserved Regulatory Networks in Human and Mouse Interneuron Development. Int J Mol Sci. 2023;24: 8122.
40. Zheng H, Liu H, Ge Y, Wang X. Integrated single-cell and bulk RNA sequencing analysis identifies a cancer associated fibroblast-related signature for predicting prognosis and therapeutic responses in colorectal cancer. Cancer Cell Int. 2021;21:108.
41. Yan T, Qiu W, Weng H, Fan Y, Zhou G, Yang Z. Single-cell transcriptomic analysis of ecosystems in papillary thyroid carcinoma progression. Front Endocrinol. 2021;12:729565.
42. Dai F, Wu J, Deng Z, Li H, Tan W, Yuan M, et al. Integrated Bioinformatic Analysis of DNA Methylation and Immune Infiltration in Endometrial Cancer. Biomed Res Int. 2022;2022:1–13.
43. Zhu J, Chen C, Li Z, Liu X, He J, Zhao Z, et al. Overexpression of Sirt6 ameliorates sleep deprivation induced-cognitive impairment by modulating glutamatergic neuron function. Neural Regen Res. 2023;18:2449–58.
44. Teng S, Zhen F, Wang L, Schalchli JC, Simko J, Chen X, et al. Control of non-REM sleep by ventrolateral medulla glutamatergic neurons projecting to the preoptic area. Nat Commun. 2022;13:4748.
45. Tucker S, Möller C, Tegerstedt K, Lord A, Laudon H, Sjödahl J, et al. The Murine Version of BAN2401 (mAb158) Selectively Reduces Amyloid-β Protofibrils in Brain and Cerebrospinal Fluid of tg-ArcSwe Mice. J Alzheimer's Dis. 2014;43:575–88.
46. Zhang Y, Ning C, Zhou H, Yan Y, Liu F, Huang Y. Interleukin-1β, interleukin-6, and interleukin-17A as indicators reflecting clinical response to celecoxib in ankylosing spondylitis patients. Irish J Med Sci (1971 -). 2020;190:631–8.
47. Zahra A, Jiang J, Chen Y, Long C, Yang L. Memantine rescues prenatal citalopram exposure-induced striatal and social abnormalities in mice. Exp Neurol. 2018;307:145–54.
48. Sun X, Li L, Dong Q-X, Zhu J, Huang Y, Hou S, et al. Rutin prevents tau pathology and neuroinflammation in a mouse model of Alzheimer's disease. J Neuroinflammation. 2021;18(1):131.

Publisher's Note